International Journal of Biological Macromolecules 292 (2025) 139278

Contents lists available at ScienceDirect

International Journal of Biological Macromolecules

journal homepage: www.elsevier.com/locate/ijbiomac

Improving fire retardancy and mechanical properties of polyurethane elastomer by acid hydrotropic lignin

Feng Gu [a,1], Wenjing Yang [a,1], Guoqing Xiao [a], Haoran Wang [a], Quan Yang [a], Zhaosheng Cai [a], Wangxia Wang [a,*], J.Y. Zhu [b,*]

[a] School of Chemistry and Chemical Engineering, Yancheng Institute of Technology, Yancheng 224051, China
[b] USDA Forest Service, Forest Products Laboratory, Madison, WI 53726, USA

ARTICLE INFO

Keywords:
Acid hydrotrope lignin
Polyurethane
Flame retardancy
Mechanical strength
Reprocessibility

ABSTRACT

Improving flame retardancy and mechanical strength of lignin-containing polyurethane is a great challenge. In this study, lignin with favorable reactivity and dispersity was extracted from poplar using acid hydrotrope *p*-TsOH in EtOH. The extracted acid hydrotrope lignin (AHL) was subsequently functionalized with nitrogen and phosphorus (FHL) and reacted with isocyanate to fabricate a fire-retardant polyurethane (FHL-PU). The resulting FHL-PU exhibited a five-fold increase in fracture toughness and remarkable reprocessability, attributable to the dual cross-linked network formed by dynamic hydrogen bonds and carbamate bonds between AHL and PU. Furthermore, the FHL can effectively prevent the release of heat and smoke through mechanisms like forming a char layer at elevated temperatures, generating non-combustible gases and sequestering free radicals. As a result, the FHL led to a reduction in the peak heat release rate and total heat release of PU from 946.8 kW/m^2 and 86.9 MJ/m^2 to 383.5 kW/m^2 and 28.4 MJ/m^2, respectively. This acid hydrotrope lignin modified polyurethane, holds tremendous potential for a wide range of practical applications.

1. Introduction

Polyurethane (PU) is synthesized through the reaction between hydroxyl groups (—OH) and isocyanate groups (—NCO). It has extensive applications in diverse fields such as insulation for electrical wires, automotive components, protective coatings, and medical devices, owing to its remarkable processability, chemical stability, weathering capabilities, and mechanical performance [1]. Unfortunately, its low flammability, along with the emission of molten droplets, smoke, and toxic gases during combustion, is a hazard to public health and safety, which limits its broader applications [2]. The Grenfell Tower fire associated with PU took place in London on June 14, 2017, resulted in the tragic loss of 71 lives. The incident is caused by the flammable polymer materials in the exterior cladding of the building that is prone to fire [3].

Lignin is the most abundant renewable aromatic material on Earth, having a distinctive network structure and plentiful functional groups. The network structure with aromatic ring gives lignin good thermal stability and the ability to carbonization to for a continuous char layer under fire, thus prevents the release of heat and smoke after ignition [4,5]. Active hydroxyl groups (phenolic & aliphatic) can participate in various chemical reactions, such as forming hydrogen bonds or reacting with other components in the polyurethane matrix. During the combustion process, these hydroxyl groups can capture free radicals, interrupting the chain reaction of combustion and thereby inhibiting the spread of the flame [6]. In recent years, lignin has been extensively researched for improving flame retardancy of various polymeric materials, such as polylactic acid (PLA), polypropylene (PP), low density polyethylene (LDPE), and PU [7]. Alkali lignin and sodium lignosulfonate coated PU foam showed enhanced flame retardance due to the formation of dense and swelling char, capturing radicals, and dilution of inert gases [8]. Lignin doped with nitrogen and phosphorus decreased the peak heat release rate (pHRR) and the peak smoke release rate (pSRR) of phenolic PU foams by 48.0 % and 53.2 %, respectively [9]. However, high loadings of technical lignin, decreased PU mechanical strength and flexibility. This is attributed to the rigid benzene ring structures of lignin, along with the relatively feeble cross-linking between lignin and isocyanate. Consequently, the synthesis of highly flame retardant lignin-based polyurethane with outstanding mechanical

* Corresponding authors.
E-mail addresses: wangwangxia@ycit.edu.cn (W. Wang), junyong.zhu@usda.gov (J.Y. Zhu).
[1] These authors contributed equally to this work.

https://doi.org/10.1016/j.ijbiomac.2024.139278
Received 11 October 2024; Received in revised form 16 December 2024; Accepted 27 December 2024
Available online 28 December 2024

properties is a great challenge.

Alkali lignin, sodium lignosulfonate, and enzymatic hydrolysis lignin, as the main technical lignin, have limited reactivity and dispersity, perhaps because these lignin products were derived from high-temperature chemical processes with great degrees of condensation. To enhance the reactivity and dispersity of technical lignin for high-performance composite material applications, several strategies have been developed to modify its molecular structure, such as solvent fractionation [10], lignin depolymerization [11], and chemical modification [12]. Liu et al. [13] obtained lignin with low molecular weight and high phenolic hydroxyl content by depolymerizing enzymatic hydrolysis lignin to improve the reactivity for producing polyurethanes. Wang et al. [14] prepared alkali lignin nanoparticles through dissolution in NaOH and dialysis to effectively control the size of lignin particles and improve the dispersion and compatibility of lignin particles in polymer matrix. However, processes for enhancing the reactivity and dispersity of lignin often require great energy consumption for extensive processing, but with low yield.

Acid hydrotrope fractionation using aromatic acid such as *p*-TsOH has been shown to have remarkable efficiency in delignification [15,16]. By subjecting the wheat straw to an aqueous *p*-TsOH treatment, approximately 53 % of lignin nanoparticles with diameters ranging from 20 to 80 nm and heights ranging from 15 to 55 nm could be successfully extracted [17]. Meanwhile, the acid hydrotropic lignin (AHL) has a high content of *β*-aryl ether (*β*-O-4) linkages, or a great number of reactive sites for cross-linking with other polymers. The exceptional dispersity and reactivity make the AHL particle ideally suited for producing advanced composite materials. In this study, ethanol (EtOH) was chosen to construct a novel EtOH/*p*-TsOH solvent for lignin fractionation instead of aqueous *p*-TsOH to reduce energy consumption in chemical recovery through distillation. There are several major advantages using EtOH, 1) EtOH/*p*-TsOH is easier to recover than aqueous *p*-TsOH because less evaporation energy is needed as ethanol has a low boiling point, thereby decreasing production cost, 2) EtOH/*p*-TsOH system exhibits lower viscosity compared to the aqueous *p*-TsOH system, which is conducive to the dissolution of lignin and facilitate higher solids biomass loading to decrease chemical application, 3) Ethanol can reduce the degradation of xylose and the formation of uronic acids, there by prevent the dissolution of hemicelluloses.

Many natural materials possess outstanding mechanical properties due to their rich and hierarchical structure [18]. For instance, spider silk has a two-phase structure formed by the biological matrix and uniformly embedded array of hydrogen bonds. The breakage and reconfiguration of dense hydrogen bonds can consume large amounts of external energy, making spider silk one of the strongest materials in nature [19]. Introducing multistage energy sacrifice bonds is an excellent choice for improving the mechanical properties of polymers [20]. Energy sacrificial bonds typically include dynamic covalent bonds and non-covalent bonds. Yang et al. [21] combined a dual dynamic network of covalent bonds and hydrogen bonds to produce PU with high tensile strength (37.1 MPa). Herein, a novel strategy was proposed aimed at integrating dynamic phenolic-carbamate bonds with hydrogen bonds into adaptable cross-linking networks for the construction of mechanically robust, fire-resistant, and reprocessable lignin-based polyurethane. The results demonstrated that the PU synthesized with FHL (FHL-PU) displayed not only better flame retardancy but also superior mechanical properties compared with PU prepared from alkali lignin (AL). Given the observed performance differences, AL was used as a control to study the influences of network structure, dispersity, and reactivity of AHL on flame retardancy and mechanical properties of lignin-based polyurethane. Meanwhile, the mechanism of dynamic phenolic-carbamate bonds cross-linking with hydrogen bonds in FHL-PU was also explored.

2. Materials and methods

2.1. Materials

Poplar sawdust was purchased from Shandong Dongxing Wood Co., Ltd., China. Ethanol (EtOH), *p*-toluenesulfonic acid (*p*-TsOH), polytetramethylethylene ether glycol (PTMEG, Mn = 2000 g/mol), dibutyltin dilaurate (DBTDL), hexamethylene diisocyanate (HDI), 37 % formaldehyde (HCHO), 9,10-dihydro-9-oxa-10-phosphaphenanthrene-10-oxide (DOPO), polyethyleneimine (PEI, Mn = 600 g/mol), sodium hydroxide (NaOH), hydrochloric acid (HCl), and *N*, *N*-Dimethylformamide (DMF) were purchased from Aladdin Reagent Co., Ltd. (Shanghai, China). All reagents were used as received without further purification.

2.2. Lignin extraction with EtOH/p-TsOH and sodium hydroxide (NaOH)

Lignin extraction with EtOH/*p*-TsOH solvent was carried out in an oil bath with *p*–TsOH concentrations at 80 wt%. 38 mL of the prepared EtOH/*p*-TsOH solvent was heated in a 150 mL flask to 80 °C, followed by adding 2 g (oven-dry weight) of 20–80 mesh Wiley-milled poplar powder. At the end of the preset reaction time of 30 min, 60 mL of hot water was added into the flask to dilute the acid concentration to terminate reaction. Water insoluble lignocellulosic solid (WIS) was separated from the spent liquor by vacuum filtration. After separation, the WIS was washed using deionized (DI) water with vacuum filtration at room temperature for solid liquid separation until the filtrate became neutral, and the spent liquor was collected to precipitate lignin. After precipitation, the EtOH/*p*-TsOH extracted AHL was obtained through centrifugation followed by freeze-drying, as shown in Fig. 1a.

As a control, AL was obtained from traditional soda pulping process. 10 g poplar saw dust and 50 mL 1 M NaOH were mixed in an autoclave. The mixture was then heated to 150 °C and kept at that temperature for 2 h. The autoclave was then placed in an ice water bath to terminate the reaction. The pH of the spent liquor was lowered to around 3 by adding 1 M HCl. The AL was precipitated from the spent liquor after standing for 30 min. The precipitated AL was separated from the acidified spent liquor by centrifugation and further purified using diluted HCl solution three times, and then freeze-dried.

2.3. Lignin functionalization

The EtOH/p-TsOH extracted lignin (AHL) together with AL was functionalized. First, dissolve 1 g of lignin powder in 20 mL of NaOH (2 %, *w/v*) solution and stir thoroughly until the lignin is completely dissolved. Then add 0.14 g of H_2O_2, 0.01 g of $FeCl_2$, 0.4 g of HCHO, and 0.4 g of polyetherimide (PEI) to the solution, and adjust the temperature to 60–90 °C and let reaction for 4–7 h. After the reaction, 2 mol/L HCl was used to adjust pH to 2–3 to precipitate the products. The sediment was washed using distilled water until the pH was neutral, and then freeze-dried to obtain N-grafted lignin (NL). Then, dissolve 1 g of NL in 6 mL DMF with the addition of 0.004 mol HCHO and 0.004 mol DOPO. Add a certain amount of 2 mol/L HCl solution to make the reaction mixture slightly acidic (pH = 3–4). After reaction for 5–8 h at 70–100 °C, DMF was removed by rotary evaporation, and the reaction products were washed repeatedly with distilled water and then freeze-dried to obtain functionalized lignin, as illustrated in Scheme S1. The funtionalized AHL and AL were labeled as FHL and FL, respectively. The influences of reaction time, temperature and chemical dosage on nitrogen and phosphor contents of lignin were investigated (Fig. S1).

2.4. Preparation of FHL-PU

Fig. 1b and Scheme S2 show the preparation route and synthesis steps of FHL-PU. FL-PU was also synthesized using FL for comparison. Table S1 illustrates the formulations of PU, FL-PU and FHL-PU. First, desired amounts of PTMEG, DMF, DBTDL and HDI were added to a

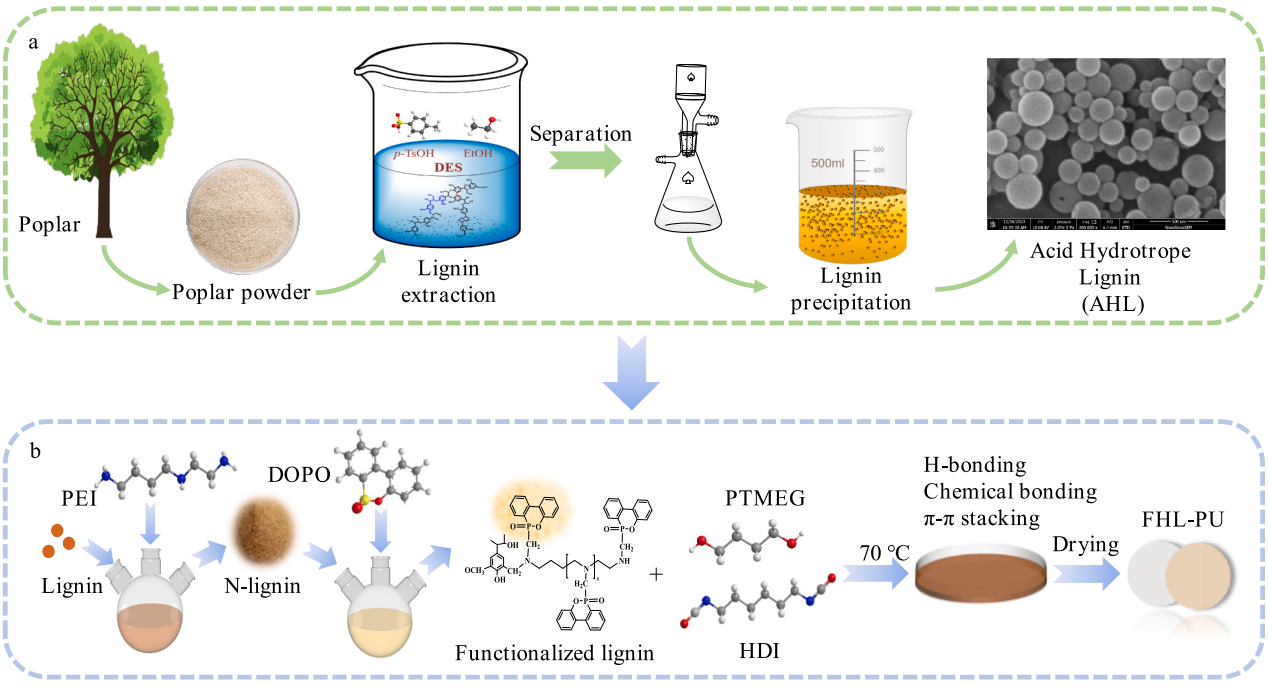

Fig. 1. The preparation route of AHL (a) and FHL-PU (b).

three-necked flask and reacted at 60 °C for 2 h to obtain PU prepolymer. The amount of HDI was calculated by hydroxyl contents in FHL and PTMEG, with a molar ratio of —NCO to —OH set at 1.1. FHL was dissolved in DMF and added to PU prepolymer at 70 °C. After 4 h reaction, the product was poured into the glass mold and dried at room temperature overnight to obtain FHL-PU.

2.5. Characterization of FHL and FHL-PU

The NMR analyses were conducted on a Bruker AVANCE III spectrometer operating at 400.13 and 100.61 MHz for ^{1}H and ^{13}C, respectively, and the obtained NMR data were processed using the TopSpin 2.1 software. 2D ^{1}H and ^{13}C HSQC spectra were acquired using spectral widths of 12 ppm for ^{1}H and 220 ppm for ^{13}C with a 2-s relaxation delay, 1 K data points, 256 t_1 increments, and 32 transients. A semi-quantification method was applied to obtain relative quantities of various lignin chemical structures based on per 100 Ar units [22] and the ^{31}P NMR was further exploited to accurately quantify the hydroxyl groups [23].

Fourier transform infrared spectroscopy (FTIR, NEXUF-670, NICOLET Inc., USA) spectra were collected between 4000 and 650 cm^{-1} wavenumbers in the attenuated total reflection (ATR) mode. To quantitatively study the effect of hydrogen bond in FHL-PU, the N—H stretching vibration bands between 3200 and 3500 cm^{-1} were divided into two absorption bands. The absorption band at 3320 cm^{-1} corresponded to the stretching vibration of hydrogen-bonded N—H groups, while the absorption band at 3440 cm^{-1} corresponded to the stretching vibration of non-hydrogen bonded N—H groups [24,25]. The degree of hydrogen bonding interaction (X_b) in the FHL-PU was calculated according to the following equation:

$$X_b = \frac{1}{1 + \frac{kS_f}{S_b}} \quad (1)$$

where S is absorption band area, subscripts b and f represent hydrogen bonding and non-hydrogen bonding, k = 3.46 [25].

Scanning electron microscopy (SEM, Nova Nano SEM 450, Frequency Electronics Inc., USA) was used to observe the micromorphology of the PUs, and all samples were sprayed with gold. The chemical states of the elements were investigated by X-ray photoelectron spectroscopy (XPS, ESCA-LAB 250 X_i, Thermo Fisher Scientific, USA) using Al K_α radiation. The thermal stability of PUs was measured using a thermogravimetric analyzer (TGA, STA 449C3/G, NETZSCH Scientific Instruments Trading Ltd., Germany) at a heating rate of 10 °C/min under a nitrogen atmosphere, and the experimental record ranges from 50 °C to 800 °C. Raman spectroscopy of char residue was performed on an Algega Dispersive Raman-Thermo Nicolet instrument (Raman, Thermo Fisher Scientific, USA) at 514 nm.

The gel fraction (G_f) and swelling ratio (S_r) of samples were calculated as follows: About 500 mg vacuum dried sample (m_0) was placed in DMF and immersed for 72 h at room temperature. Then the swelling sample was obtained after removing solvent from the surface, and the weight was recorded as m_1. Finally, the swelling sample was dried under vacuum at 80 °C for 24 h, and the weight was recorded as m_2. The gel fraction and swelling ratio were calculated by the following equations:

$$G_f = 100\% \times \frac{m_2}{m_0} \quad (2)$$

$$S_r = \frac{\frac{m_0}{\rho_0} + \frac{m_1 - m_0}{\rho_s}}{\frac{m_0}{\rho_0}} \quad (3)$$

where G_f is the gel fraction, S_r is the swelling ratio, ρ_s *and* ρ_0 (g/cm^3) is the density of DMF and PU at room temperature, m_0 is the original mass of samples, m_1 is the mass of swelling samples after infiltration, and m_2 is the swelling mass of samples after drying [26].

Mechanical property of PU, FL-PU and FHL-PU were measured by SANS Model E40 electronic universal testing machine (Metus Industrial Systems Co., LTD, USA) equipped with a 500 N load cell at a cross-head speed of 100 mm/min according to ISO 37:2005. Flame retardancy of specimen (100 mm × 100 mm × 3 mm) was evaluated using a cone calorimeter (VOUCH-6810, Suzhou Yangyi Volki Testing Technology Co., LTD, China) according to ISO 5660-1: 2002 with an incident flux of 50 kW/m^2. The limiting oxygen index (LOI) of FHL-PU was measured according to the oxygen index method (ASTM D2863) by a limiting oxygen index instrument (ZR-01, Qingdao Shanfang Instrument Co., ltd., China). The UL-94 vertical burning tests were conducted according

to the UL-94 standard (ASTM D3801) with a sample dimension of 80 mm × 6.5 mm × 3 mm on a vertical burning test instrument (M601, Qingdao Shanfang Analysis Instrument Co., ltd., China). Duplicate runs of each test were carried out and the averages were reported.

3. Results and discussion

3.1. Structural analysis of EtOH/p-TsOH extracted lignin (AHL) and alkaline lignin (AL)

The yield of AHL extracted using EtOH/*p*-TsOH at 80 °C for 30 min reached 72.6 %, whereas the yield of AL extracted using 1 M NaOH at 150 °C for 2 h was 36.2 %. Fig. 2 presents the 2D NMR spectral features of side chain ($\delta C/\delta_H$ 50–95/2.5–6.0 ppm) and aromatic regions ($\delta C/\delta_H$ 95–140/6.0–8.0 ppm) of the AHL and AL. The result shows that AHL has the typical characteristics of hardwood lignin. Solvent EtOH/*p*-TsOH preserved the structure of the lignin and maintained 42.4 % of *β*-O-4 bonds in the lignin. The content of *β*-O-4 bonds is positively correlated with the integrity of the lignin structure. Higher amounts of *β*-O-4 result in a more robust network structure. Compared to AHL, the disappearance of *α*, *β*-position signals of side chain region and unknown signals of aromatic region in AL indicates that soda cooking resulted in more *β*–O–4 linkage cleavage than EtOH/*p*-TsOH cooking. ^{31}P NMR was used to accurately quantify the hydroxyl groups in the AHL and AL, as shown in Table 1. The AL contains fewer alcoholic hydroxyl group and more phenolic hydroxyl group than AHL, indicating that more *β*-O-4 cleavage and condensation of lignin occurred during soda cooking. The phenolic hydroxyl group content in AL is much higher than that in AHL. However, flame retardant modification mainly occurs on the *α*-H of G phenolic hydroxyl groups. Overall, the EtOH/*p*-TsOH solvent system can maintain the excellent dispersion (See SEM image in Fig. 1) and structural integrity of AHL at a relatively high extraction yield, which is benefit for the subsequent valorization of lignin.

3.2. Characterizations of FHL

FTIR and XPS are employed to explore the FHL surface chemical structure. The FHL showed C—N stretching vibration at 1655 cm^{-1}. The band at 1200 cm^{-1} was the combination of the stretching and bending vibrations of the P═O bond, the band at 1050 cm^{-1} was the stretching vibrations of the P—O bond [27], and the absorption band at 760 cm^{-1} was attributed to the stretching vibrations of P—N—C (Fig. 3a). XPS spectra explored the constituents of FHL's chemical state and composition (Fig. 3b). The peaks observed at 533, 400, 286, 195, and 137 eV were attributed to O1s, N1*s*, C1s, P2s, and P2p, respectively. For the O1s spectrum (Fig. S2a), three peaks at 533.0 eV (C═O), 532.0 eV (C—O) and 530.6 eV (P—O or P═O) were observed. Peaks at 401.9, 401.5, and 399.8 eV make up the N1*s* spectra (Fig. S2b). These peaks belonged to the groups of N—H, C—N, and N—P. Three peaks at 285.8 eV (C—O), 284.7 eV (C—N) and 284.1 eV (C═C or C—C) make up the C1*s* spectra (Fig. S2c). In the P2p spectrum (Fig. S2d), two peaks at 133.5 eV and 132.3 eV were also noted, which were assigned to P═O and O—P—N, respectively [28]. The above analysis confirmed that FHL has been successfully functionalized with nitrogen and phosphor.

Thermal stability is a crucial indicator of the fire performance of FHL. As shown in Fig. 3c and d, the initial weight loss temperature (T_i) and the maximum weight loss temperature (T_{max}) of AHL are 250.5 °C and 368.3 °C, respectively. After nitrogen- and phosphorus-functionalization, the T_i and T_{max} of FHL increased to 313.0 °C and 391.3 °C, respectively. Furthermore, the carbon residue of FHL increased to 47.5 % at 800 °C under the nitrogen atmosphere, indicating that the thermal stability of FHL has been improved. The decomposed phosphoric acid groups on FHL can promote lignin dehydration and thus increase the FHL carbonization [29].

3.3. Synthesis and characterization of PU, FL-PU and FHL-PU

The FTIR spectra of PU, FL-PU and FHL-PU are presented in Fig. 4a. The infrared bands observed at 3440 and 3320 cm^{-1} correspond to the N—H stretching modes of the "free" (non-hydrogen bonded) and hydrogen bonded N—H groups within the polyurethane structure, respectively. Notably, the band at 3320 cm^{-1} mainly reflects the distribution of hydrogen bond strengths [24]. To calculate the degree of hydrogen bonding interaction in FHL-PU, the infrared bands within the 3100–3600 cm^{-1} range were divided into two bands, as illustrated in Fig. S3. It was found that FHL-PU has a higher content of hydrogen bonded N—H groups compared with FL-PU. The infrared band at 1680–1720 cm^{-1} region is assigned to carbonyl stretching vibration contributed by the ordered H-bonded carbonyl groups at 1680 cm^{-1}, disordered H-bonded carbonyl groups at 1615 cm^{-1}, and free carbonyl

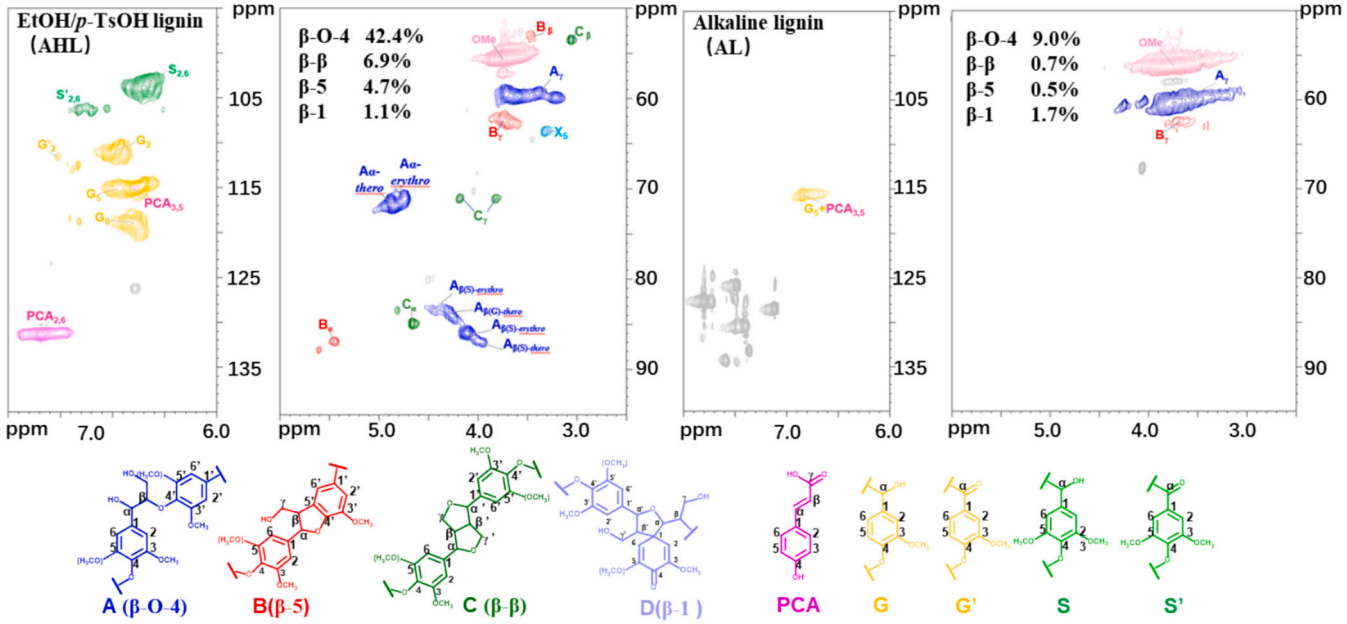

Fig. 2. Aromatic and side chain region in the 2D HSQC NMR of the AHL and AL from poplar.

Table 1
Hydroxyl contents of AHL and AL determined by ^{31}P NMR.

Sample	Hydroxyl content, mmol/g					
	Total	Alcoholic	Condensed phenolic unit	Syringyl phenolic unit	Guaiacyl phenolic unit	Carboxylic acid
AHL	5.22 ± 0.07	3.94 ± 0.07	0.18 ± 0.01	0.43 ± 0.04	0.60 ± 0.04	0.08 ± 0.01
AL	4.78 ± 0.09	1.08 ± 0.05	0.98 ± 0.04	1.84 ± 0.08	0.78 ± 0.03	0.11 ± 0.01

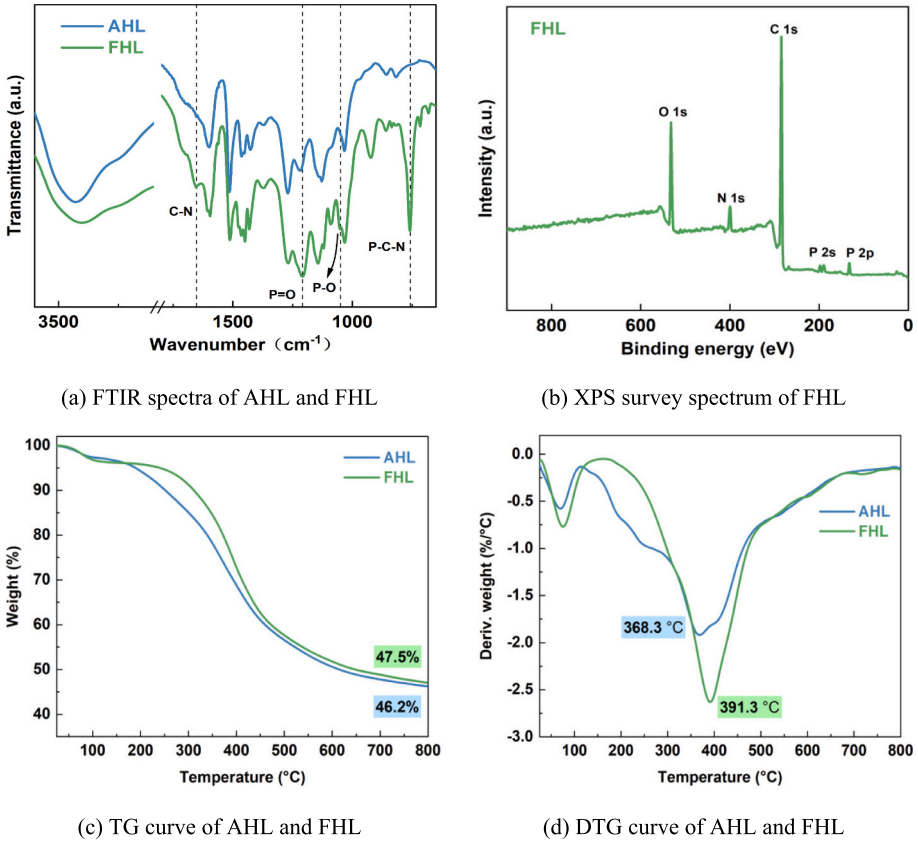

(a) FTIR spectra of AHL and FHL

(b) XPS survey spectrum of FHL

(c) TG curve of AHL and FHL

(d) DTG curve of AHL and FHL

Fig. 3. FTIR spectra (a), XPS spectra (b), TGA curves (c) and DTG curves (d) of AHL and FHL.

groups at 1715 cm^{-1} [24]. Compared with FL-PU, the intensity of the infrared band corresponding to C═O in FHL-PU at 1680 cm^{-1} was enhanced. The enhancement indicates the formation of ordered H-bonded carbonyl groups by FHL addition, which leads to a blue shift of the carbonyl absorbance bands upon the addition of lignin [30,31]. The greater content of hydrogen bonded N—H groups and ordered H-bonded carbonyl groups by FHL addition indicate that the —OH in FHL interacts with the PU chain to form hydrogen bond networks. This can be beneficial from improving the mechanical properties of the composites [21,31].

3.4. Mechanical properties of PU, FL-PU and FHL-PU

The degree of dynamic cross-linking between lignin and PU matrix will directly determine the strength and flexibility of FHL-PU. As depicted in Fig. 4a and b, the greater content of hydrogen-bonded N—H groups and the ordered H-bonded carbonyl groups in FHL-PU resulted in enhanced cross-linking between lignin and PU formed by carbamate bonds and hydrogen bonds. This is because the unesterified hydroxyl group in the extracted AHL can interact with the hydroxyl and carbonyl group of prepolymers to result in a much denser cross-linking structure through dynamic non-covalent interactions and covalent linkages. The rupture of hydrogen bonds during tension leads to energy dissipation [33]. This phenomenon boosts the tensile strength of FHL-PU to 35.8 MPa and extends the strain to 1289 %, with a fracture toughness reaching 178.7 MJ/m^3, significantly greater than the corresponding values for lignin-based polyurethane elastomers prepared using sequential precipitated kraft lignin (LLPU2) [34], oleic acid esterified organosolv lignin (LPU-5) [35], hydrothermal degraded acetic acid lignin (DAAL-PUE) [36], and depolymerized enzymatic hydrolysis residue lignin (20 % DEL) [13], as illustrated in Table 2. Moreover, AHL with a higher β-O-4 content exhibits a more intact network structure in comparison to AL. This structure enables lignin to enhance the strength and flexibility of lignin-based polyurethane materials through mechanisms such as providing a rigid supporting framework, improving stress transfer efficiency, and inducing the formation of microphase separation structure [37]. Furthermore, SEM image shows the FHL particles can be well dispersed and embedded in PU matrix (Fig. 4e). The increase in gel fraction and swelling ratio (Fig. S4) indicates the enhanced intermolecular interaction between FHL and PU [14,32]. Specifically, the tensile strengths of FL-PU and FHL-PU are 22.0 MPa and 35.8 MPa, respectively, in contrast to 7.2 MPa of PU (Fig. 4b).

3.5. Flame retardancy of PU, FL-PU and FHL-PU

Like other polyurethane materials, thermal degradation of PU occurred in two stages at 300–350 °C and 350–480 °C (Fig. 5a & b). The first stage is mainly related to the degradation of the hard constituents

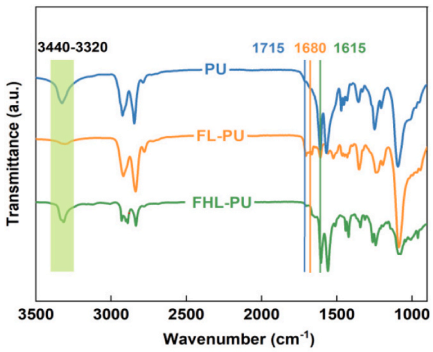

(a) FTIR spectra of PU, FL-PU and FHL-PU

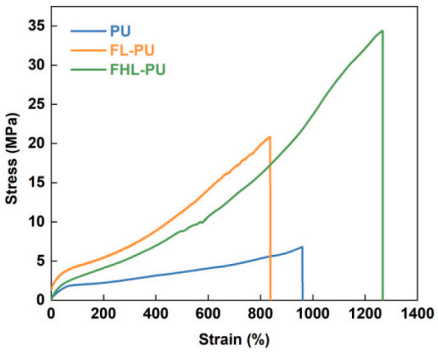

(b) Stress-strain curves of PU, FL-PU and FHL-PU

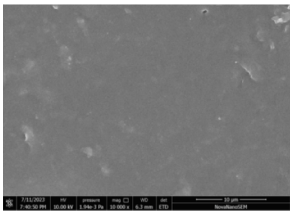

(c) SEM image of PU

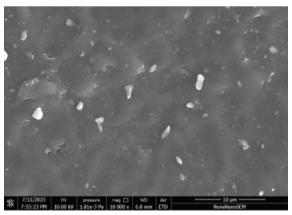

(d) SEM image of FL-PU

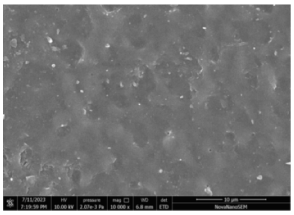

(e) SEM image of FHL-PU

Fig. 4. FTIR spectra (a), Stress-strain curves (b) and SEM images (c, d, e) of PU, FL-PU and FHL-PU.

Table 2
Mechanical properties and flame retardancy of lignin-based PU.

Sample	Lignin	Functionalization	Tensile strength (MPa)	Strain (%)	Toughness (MJ/m^2)	pHRR (kW/m^2)	THR (MJ/m^2)	Reference
FHL-PU	Acid hydrotropic lignin	N/P	35.8	1289	178.7	383.5	28.4	This work
LLPU2	Kraft lignin	Sequential precipitation	32.8	34.5	~5			[34]
LPU-5	Organosolv lignin	Oleic acid esterification	9.6	181	~8			[35]
DAAL-PUE	Acetic acid lignin	Hydrothermal degradation	28.9	960	~133			[36]
20 % DEL	Enzymatic hydrolysis lignin	Depolymerization	38.8	950.8	157			[13]
0.5-OL$_{20}$PU	Organosolv lignin	Ozone Oxidation	47.2	120	~5			[1]
L0.5P9.5 T0.2	Alkaline lignin	Organic solvent extraction	14.2	1540	103.3			[7]
TPU/3C-P-Lignin	Kraft lignin	PSPD/DMOA	28.3	941	139	607	~70	[38]
PUE/15-Nano-FL	Acetic acid lignin	N/P	47.5	920	~175	370	70.7	[39]
PU-PL25	Kraft lignin	Phosphorylation				361.5	99.4	[40]
PUE6	Low-sulfonated alkaline lignin	Ammonium polyphosphate				341	124	[41]

(isocyanate) and the second stage is associated with the degradation of the soft constituents (polyol) [30]. The initial degradation temperature (T_i) of PU was 289.2 °C, and the two maximum destruction temperatures were 318.2 °C and 421.8 °C, respectively. As the data show, due to the addition of FHL particles to the polyurethane matrix, the T_{max} of FHL-PU was decreased to 396.5 °C (Table 3). The introduction of N/P-functionalized lignin alters the original thermal stability of PU. At relatively low temperatures, P-containing groups start to decompose and release acidic substances. These acidic substances can catalyze the breaking of chemical bonds within lignin molecules and trigger lignin thermal decomposition prematurely. As the temperature increases, the main chain of lignin further decomposes under the combined influence of acidic substances and heat. During the process, the decrease in free radicals by N suppressed combustion chain reaction. P promoted lignin cross-linking, leading to small molecular fragment aggregation and carbonaceous structure formation. At high temperatures, thermal decomposition stabilizes due to the formation of a stable carbon layer, a key product from N/P-functionalized lignin decomposition which has good heat insulation and prevented heat transfer and oxygen ingress, and therefore inhibited material combustion [42,43].

To assess the flame retardancy of PU, FL-PU and FHL-PU, their peak heat release rate (pHRR), total heat release (THR), smoke production rate (SPR) and total smoke production (TSP) values were measured using a cone calorimeter (Fig. 5c–f). Compared with PU, FHL-PU exhibited a significant decrease of 59.5 % in the pHRR. Specifically, the pHRR of PU was 946.8 kW/m^2, whereas FHL-PU exhibited a pHRR of 383.5 kW/m^2 and FL-PU had a pHRR of 672.1 kW/m^2. This is in agreement with literature value of 607 kW/m^2 from PU synthesized with phenyl dichloro sphosphineoxid and 1, 4-dimethoxyacetylene functionized alkali lignin [38]. The THR of FHL-PU was substantially lower at 28.4 MJ/m^2 compared with 86.9 MJ/m^2 for PU, representing a decrease of 67.3 %. It is also lower than the 70.7 MJ/m^2 for PU

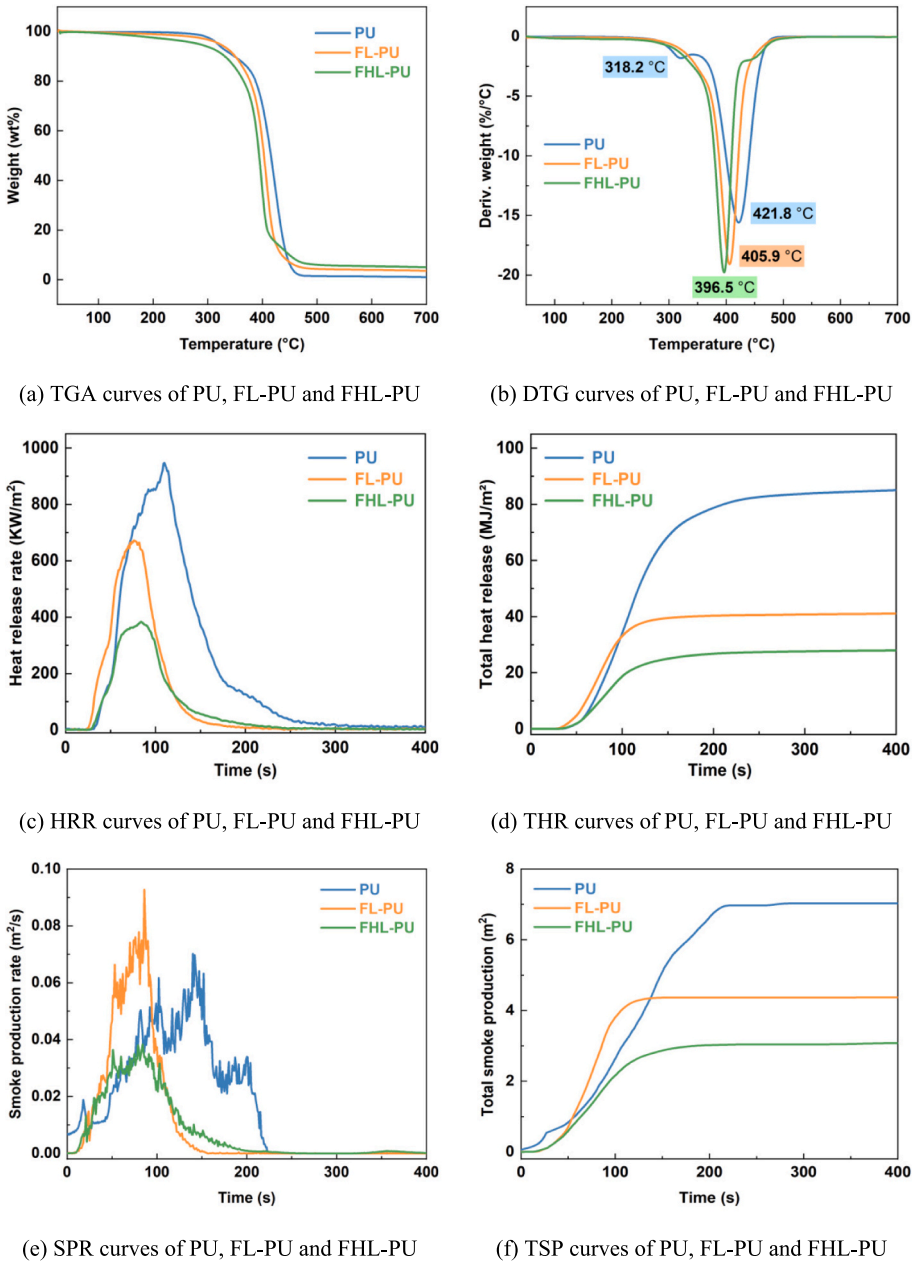

(a) TGA curves of PU, FL-PU and FHL-PU

(b) DTG curves of PU, FL-PU and FHL-PU

(c) HRR curves of PU, FL-PU and FHL-PU

(d) THR curves of PU, FL-PU and FHL-PU

(e) SPR curves of PU, FL-PU and FHL-PU

(f) TSP curves of PU, FL-PU and FHL-PU

Fig. 5. TGA curves (a), DTG curves (b), HRR curves (c), THR curves (d), SPR curves (e), and TSP curves (f) of PU, FL-PU and FHL-PU.

Table 3
TG analysis results of PU, FL-PU and FHL-PU.

Sample	T_i (°C)	T_{max1} (°C)	T_{max2} (°C)	Residue (wt%)
PU	289.2	318.2	421.8	1.1
FL-PU	381.7	405.9	–	3.6
FHL-PU	374.1	396.5	–	5.0

Table 4
Cone calorimetry test data of PU, FL-PU and FHL-PU.

Sample	pHRR (kW/m²)	THR (MJ/m²)	pSPR (m²/s)	TSP (m²)	FSI (kW/m²/s)
PU	946.8 ± 32.6	86.9 ± 1.2	0.07 ± 0.02	7.0 ± 1.1	8.6 ± 0.3
FL-PU	672.1 ± 36.1	41.8 ± 0.9	0.09 ± 0.02	4.4 ± 0.8	8.8 ± 0.5
FHL-PU	383.5 ± 27.6	28.4 ± 1.1	0.04 ± 0.01	3.1 ± 0.9	4.6 ± 0.3

synthesized with N/P-functionalized acetic acid lignin nanoparticles [39]. The pSPR and TSP were reduced from 0.07 m^2/s and 7.0 m^2 to 0.04 m^2/s and 3.1 m^2, respectively (Table 4). To further evaluate the flame retardancy of FHL-PU, the LOI test and vertical burning test were performed. PU was flammable, accompanied by molten droplets with LOI value of 18.3 %. The molten droplets can easily ignite cotton, which could cause serious secondary hazards in real fires (Fig. 6a). FHL-PU has a remarkably short self-extinguishing time of 2 s (Table S2) with an LOI value of 30.2 % and achieved a vertical burning rating of *V*-0, clearly demonstrates its outstanding flame retardant performance. FHL-PU also has a remarkable anti-dripping ability after combustion, which is presumably attributable to the hydrogen bonding and π-π stacking interactions within FHL-PU. These interactions effectively limit the movement of molecular chains, leading to a substantial increase in molten viscosity [44,45]. As a consequence, the generation of molten

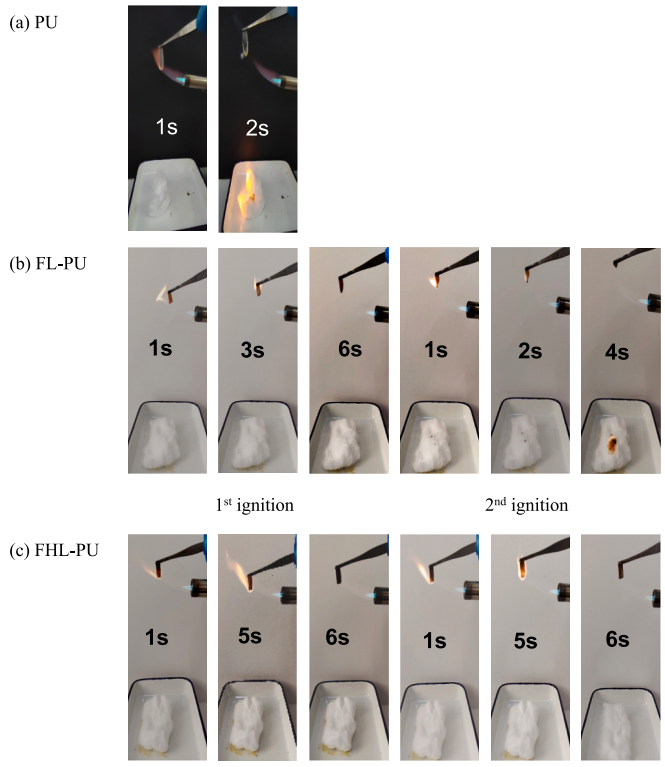

Fig. 6. Burning test of PU, FL-PU and FHL-PU.

droplets was postponed, affording the FHL-PU polymers sufficient time for the carbonization process to take place, thereby signifying an enhanced anti-dripping performance of the polyurethane.

Fire Spread Index (FSI) is an important indicator of fire risk, which is defined as the ratio of pHRR to TpHRR (time to pHRR) [46]. The lower the FSI value, the lesser the fire risk. The FSI of the pure PU is 8.6 kW/m^2/s, compared with 4.6 kW/m^2/s for FHL-PU as the lowest among all PU elastomer.

3.6. Flame-retardant mechanism

The improvement in the flame retardancy of PU by the addition of N/P-functionalized lignin is primarily attributed to the increasing formation of a highly graphitized char layer during FHL-PU combustion. The cone calorimeter tests on the condensed phases of PU revealed minimal amounts of char residue that was fragmented, discontinuous, and riddled with numerous holes (Fig. S5a & b). However, with the incorporation of FHL, the char layer expanded rapidly. Notably, the amount of char residue from FHL-PU increased substantially (Fig. S5d & e). The SEM morphology also showed that the addition of FHL resulted in a denser and more intact char residue (Fig. S5c & f). The degrees of graphitization of the PU and FHL-PU residues were determined by calculating the area ratio of *D* to G peaks (I_D/I_G) of the Raman spectra (Fig. 7a). The I_D/I_G value of PU was 3.9, while that of FHL-PU was 3.2. Generally, a lower I_D/I_G indicates a higher degree of graphitization [47,48]. To gain further insights into the combustion process, the types of chemical bonds in the char residue were analyzed using FTIR (Fig. 7b). The absorption band at 1600 cm^{-1} corresponded to the stretching vibration of C═C in the benzene rings of FHL, along with characteristic absorption bands of aromatic rings at 1450 and 1380 cm^{-1} [6]. Additionally, the FHL-PU exhibited stretching vibrations of the P═O band at 1200 cm^{-1} and P—O at 1010 cm^{-1}. The band at 760 cm^{-1} also signified the presence of P—N—C in the char residues of FHL-PU [27].

This enhanced generation of the highly graphitized char layer is a consequence of the synergistic effect of phosphorus and nitrogen. Phosphorus facilitates cross-linking reactions via the formation of bonds such as P—O—C or P—O—P and drives the graphitization process by reducing the activation energy required for carbon rearrangement. Nitrogen, on the other hand, scavenges free radicals, thereby halting further chain reactions and oxidative degradation. Nitrogen also gets incorporated into the graphitic structure, modifying its electronic characteristics and enhancing its stability. The combined and reinforcing interaction between N and P fortifies the char layer with greater resistance to oxidation and improved thermal conductivity, which ultimately led to the formation of a highly graphitized char layer [38,49]. This cross-linked, highly carbonized aromatic network functions as an effective barrier, safeguarding the polymer from degradation at elevated temperatures and impeding the transfer of heat and oxygen.

Apart from char layer formation, free-radical scavenging also contributes to the improvement of flame retardancy. The N element in FHL can generate nitrogen-based radicals during combustion. These N-based radicals can react with active radicals generated during combustion, to interrupt the free-radical chain reaction and inhibit combustion. The P element also generates P-based radicals during combustion which have a strong oxygen-capturing ability, to decrease oxygen supply to the combustion process and slow down the burning rate. During combustion, N/P-modified lignin may decompose to produce some non-flammable gases, such as nitrogen, carbon dioxide, and water vapor, which can dilute oxygen concentrations, decrease combustion intensity

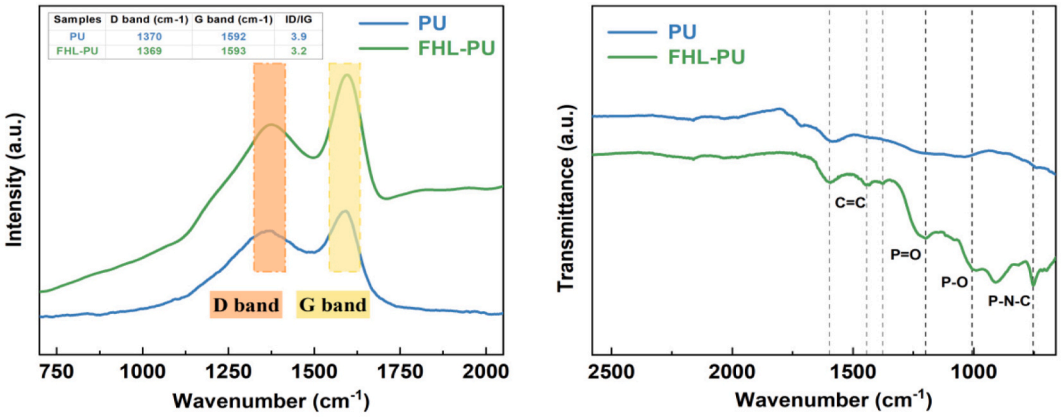

(a) Raman spectra (b) FTIR spectra

Fig. 7. Raman and FTIR spectra of PU and FHL-PU after combustion.

[50,51]. The synergistic effect of char layer formation, free-radical scavenging and non-flammable gases production during FHL-PU combustion contributes to the improvement of flame retardancy.

3.7. Reprocessability of FHL-PU

Based on the dynamically reversible property of phenol-carbamate bonds, the reprocessability of lignin-based polyurethane was investigated. The FHL-PU was cut into small pieces and placed in the mold for hot pressing (160 °C), as depicted in Fig. S6. The reprocessability of FHL-PU was mainly attributed to the transesterification reaction of carbamate bonds at high temperature, which restored the damaged covalent cross-linking network of FHL-PU. In addition, hydrogen bonds were disrupted and reestablished, further enhancing the reprocessability of FHL-PU. This reproducible property provided a new possibility for the recycling of lignin-based polyurethane.

Although N/P functionalized lignin shows certain effectiveness in enhancing the flame retardancy of polyurethane, it also has several limitations. Bio-based lignin inherently lacks essential flame-retardant properties. Even after modification, the degree of flame retardancy improvement may not meet the stringent requirements for some high-risk fire scenarios. The modification process often demands precise control and specific reagents, which can be time-consuming and costly, thereby restricting its widespread industrial adoption. Additionally, excessive addition to achieve better flame retardancy might lead to a decrease in the strength and toughness of the final material, compromising its overall performance. There is also a concern regarding the durability of the flame-retardant effect. Over time and under various environmental stresses like temperature fluctuations and humidity, the flame-retardant performance may deteriorate, compromising the long-term safety and reliability of the polyurethane materials in practical use.

4. Conclusions

Through the construction of a dynamic cross-linking network, acid hydrotrope lignin (AHL)-based polyurethane, possessing enhanced fire resistance, mechanical properties, and reprocessibility, was successfully fabricated. The fracture toughness of FHL-PU was enhanced to 178.7 MJ/m^3, a five-fold increase over that of PU. This effectively overcomes the mechanical performance deficiencies typically associated with conventional lignin-based PU. The peak heat release rate (pHRR) and total heat release (THR) of FHL-PU were remarkably diminished by 59.5 % and 67.3 %, respectively. The synergistic effect of char layer formation, free-radical scavenging and non-flammable gases production during FHL-PU combustion contributes to the improvement of flame retardancy. This approach presents a sustainable pathway for the development of lignin-based functional materials.

CRediT authorship contribution statement

Feng Gu: Writing – original draft, Methodology, Investigation, Formal analysis, Data curation, Conceptualization. **Wenjing Yang:** Writing – original draft, Methodology, Investigation, Data curation, Conceptualization. **Guoqing Xiao:** Formal analysis, Data curation. **Haoran Wang:** Formal analysis, Data curation. **Quan Yang:** Formal analysis, Data curation. **Zhaosheng Cai:** Writing – review & editing, Supervision. **Wangxia Wang:** Writing – review & editing, Supervision, Conceptualization. **J.Y. Zhu:** Writing – review & editing, Supervision, Conceptualization.

Declaration of competing interest

The authors declare that they have no known competing financial interests or personal relationships that could have appeared to influence the work reported in this paper.

Acknowledgments

We acknowledge the financial support from National Natural Science Foundation of China (No. 21908188, 22008206 & 32071706), Natural Science Foundation of Jiangsu Province (No. BK20181051 & BK20181052) and Key Research and Development Programs of Yancheng City (No. YCBE202249).

Appendix A. Supplementary data

Supplementary data to this article can be found online at https://doi.org/10.1016/j.ijbiomac.2024.139278.

Data availability

The datasets generated during and analyzed during the current study are available from the corresponding author on reasonable request.

References

[1] Y. Zhang, R. Yan, T.D. Ngo, Q. Zhao, J. Duan, X. Du, Y. Wang, B. Liu, Z. Sun, W. Hu, H. Xie, Ozone oxidized lignin-based polyurethane with improved properties, Eur. Polym. J. 117 (2019) 114–122, https://doi.org/10.1016/j.eurpolymj.2019.05.006.
[2] S. Liu, C. Kuan, C. Ke, M. Shen, C. Chiang, A novel effective halogen-free biomass-based chitosan derived flame retardant through microencapsulation technology for improved flame retardancy, thermal stability of polyurethane, Polym. Degrad. Stab. 219 (2024) 110604, https://doi.org/10.1016/j.polymdegradstab.2023.110604.
[3] Z. Ma, X. Liu, X. Xu, L. Liu, B. Yu, C. Maluk, G. Huang, H. Wang, P. Song, Bioinspired, highly adhesive, nanostructured polymeric coatings for superhydrophobic fire-extinguishing thermal insulation foam, ACS Nano 15 (2021) 11667–11680, https://doi.org/10.1021/acsnano.1c02254.
[4] Y. Guo, C. Cheng, T. Huo, Y. Ren, X. Liu, Highly effective flame retardant lignin/polyacrylonitrile composite prepared via solution blending and phosphorylation, Polym. Degrad. Stab. 181 (2020) 109362, https://doi.org/10.1016/j.polymdegradstab.2020.109362.
[5] C.R. Correa, M. Stollovsky, T. Hehr, M. Rauscher, B. Rolli, A. Kruse, Influence of the carbonization process on activated carbon properties from lignin and lignin-rich biomasses, ACS Sus. Chem. Eng. 5 (2017) 8222–8233, https://doi.org/10.1021/acssuschemeng.7b01895.
[6] L. Liu, L. Qian, P. Song, G. Huang, Y. Yu, S. Fu, Fabrication of green lignin-based flame retardants for enhancing the thermal and fire retardancy properties of polypropylene/wood composites, ACS Sus. Chem. Eng. 4 (2016) 2422–2431, https://doi.org/10.1021/acssuschemeng.6b00112.
[7] H. Wang, J. Huang, W. Liu, J. Huang, D. Yang, X. Qiu, J. Zhang, Tough and fast light-controlled healable lignin-containing polyurethane elastomers, Macromolecules 55 (2022) 8629–8641, https://doi.org/10.1021/acs.macromol.2c01401.
[8] D. Zhang, J. Zeng, W. Liu, X. Qiu, Y. Qian, H. Zhang, Y. Yang, M. Liu, D. Yang, Pristine lignin as a flame retardant in flexible PU foam, Green Chem. 23 (2021) 5972–5980, https://doi.org/10.1039/d1gc01109j.
[9] S. Weng, Z. Li, C. Bo, F. Song, Y. Xu, L. Hu, Y. Zhou, P. Jia, Design lignin doped with nitrogen and phosphorus for flame retardant phenolic foam materials, React. Funct. Polym. 185 (2023) 105535, https://doi.org/10.1016/j.reactfunctpolym.2023.105535.
[10] J.S. Rodrigues, V. Lima, L.C.P. Araújo, V.R. Botaro, Lignin fractionation methods: can lignin fractions be separated in a true industrial process, Ind. Eng. Chem. Res. 60 (2021) 10863–10881, https://doi.org/10.1021/acs.iecr.1c01704.
[11] N. Zhou, W. Thilakarathna, Q. He, H. Rupasinghe, A review: Depolymerization of lignin to generate high-value bio-products: opportunities, challenges, and prospects, Front. Energy Res. 9 (2022) 1–18, https://doi.org/10.3389/fenrg.2021.758744.
[12] A.E. Kazzaz, P. Fatehi, Technical lignin and its potential modification routes: a mini-review, Ind. Crop. Prod. 154 (2020) 112732, https://doi.org/10.1016/j.indcrop.2020.112732.
[13] W. Liu, C. Fang, S. Wang, J. Huang, X. Qiu, High-performance lignin-containing polyurethane elastomers with dynamic covalent polymer networks, Macromolecules 52 (2019) 6474–6484, https://doi.org/10.1021/acs.macromol.9b01413.
[14] H. Wang, D. Zhu, W. Liu, J. Huang, J. Huang, D. Yang, X. Qiu, Strong and tough lignin-containing waterborne polyurethane nanocomposites with multiple hydrogen bonds as photothermal power generation coatings, ACS Sus. Chem. Eng. 11 (2023) 17142–17156, https://doi.org/10.1021/acssuschemeng.3c05634.
[15] L. Chen, J. Dou, Q. Ma, N. Li, R. Wu, H. Bian, D. Yelle, T. Vuorinen, S. Fu, X. Pan, J. Y. Zhu, Rapid and near-complete dissolution of wood lignin at ≤80 degrees C by a recyclable acid hydrotrope, Sci. Adv. 3 (2017) e1701735, https://doi.org/10.1126/sciadv.17017.
[16] J.Y. Zhu, L. Chen, C. Cai, Acid hydrotropic fractionation of lignocelluloses for sustainable biorefinery: advantages, opportunities, and research needs, ChemSusChem 14 (2021) 3031–3046, https://doi.org/10.1002/cssc.202100915.

[17] W. Wang, F. Gu, J.Y. Zhu, K. Sun, Z. Cai, S. Yao, W. Wu, Y. Jin, Fractionation of herbaceousbiomass using a recyclable hydrotropic p–toluenesulfonic acid (p–TsOH)/choline chloride (ChCl) solvent system at low temperatures, Ind. Crop Prod. 150 (2020) 112423.
[18] M.S. Ganewatta, Z. Wang, C. Tang, Chemical syntheses of bioinspired and biomimetic polymers toward biobased materials, Natur. Rev. Chem. 5 (2021) 753–772, https://doi.org/10.1038/s41570-021-00325-x.
[19] S. Keten, Z. Xu, B. Ihle, M.J. Buehler, Nanoconfinement controls stiffness, strength and mechanical toughness of beta-sheet crystals in silk, Nat. Mater. 9 (2010) 359–367, https://doi.org/10.1038/nmat2704.
[20] X. Liu, X. Liu, W. Li, Y. Ru, Y. Li, A. Sun, L. Wei, Engineered self-healable elastomer with giant strength and toughness via phase regulation and mechano-responsive self-reinforcing, Chem. Eng. J. 410 (2021) 128300, https://doi.org/10.1016/j.cej.2020.128300.
[21] S. Yang, S. Wang, X. Du, Z. Du, X. Cheng, H. Wang, Mechanically robust self-healing and recyclable flame-retarded polyurethane elastomer based on thermoreversible crosslinking network and multiple hydrogen bonds, Chem. Eng. J. 391 (2020) 123544, https://doi.org/10.1016/j.cej.2019.123544.
[22] H. Wang, H. Qiao, J. Guo, J. Sun, H. Li, S. Zhang, X. Gu, Preparation of cobalt-based metal organic framework and its application as synergistic flame retardant in thermoplastic polyurethane (TPU), Compos. Part B Eng. 182 (2020) 107498, https://doi.org/10.1016/j.compositesb.2019.107498.
[23] A. Granata, D.S. Argyropoulos, 2-Chloro-4,4,5,5-tetramethyl-1,3,2-dioxaphospholane, a reagent for the accurate determination of the uncondensed and condensed phenolic moieties in lignins, J. Agr. Food Chem. 43 (1995) 1538–1544, https://doi.org/10.1021/jf00054a023.
[24] M.M. Coleman, K.H. Lee, D.J. Skrovanek, C.P. Painter, Hydrogen bonding in polymers. 4. Infrared temperature studies of a simple polyurethane, Macromolecules 19 (1986) 2149–2157, https://doi.org/10.1021/ma00162a008.
[25] V.W. Srichatrapimuk, S.L. Cooper, Infrared thermal analysis of polyurethane block polymers, J. Macromol. Sci. B 15 (2006) 267–311, https://doi.org/10.1080/00222347808212599.
[26] J. Huang, H. Wang, W. Liu, J. Huang, D. Yang, X. Qiu, L. Zhao, F. Hu, Y. Feng, Solvent-free synthesis of high-performance polyurethane elastomer based on low-molecular-weight alkali lignin, Int. J. Biol. Macromol. 225 (2023) 1505–1516, https://doi.org/10.1016/j.ijbiomac.2022.11.207.
[27] Y. Yu, S. Fu, P.A. Song, X. Luo, Y. Jin, F. Lu, Q. Wu, J. Ye, Functionalized lignin by grafting phosphorus-nitrogen improves the thermal stability and flame retardancy of polypropylene, Polym. Degrad. Stab. 97 (2012) 541–546, https://doi.org/10.1016/j.polymdegradstab.2012.01.020.
[28] P. Zhao, W. Zeng, Z. Yang, Y. Yang, J. Li, J. Shi, N. Wen, H. Li, J. Guan, Z. Lei, D. Chen, Preparation of a novel functionalized magnesium-based curing agent as an intrinsic flame retardant for epoxy resin, Chemosphere 273 (2021) 129658, https://doi.org/10.1016/j.chemosphere.2021.129658.
[29] S. Chen, H. Li, X. Lai, S. Zhang, X. Zeng, Superhydrophobic and phosphorus-nitrogen flame-retardant cotton fabric, Prog. Org. Coat. 159 (2021) 106446, https://doi.org/10.1016/j.porgcoat.2021.106446.
[30] Z. Huang, H. Wang, J. Du, X. Liu, G. Pan, X. Yin, W. Lin, X. Lin, Y. Sun, G. Yi, L. Niu, High-strength, self-reinforcing and recyclable multifunctional lignin-based polyurethanes based on multi-level dynamic cross-linking, Chem. Eng. J. 473 (2023) 145423, https://doi.org/10.1016/j.cej.2023.145423.
[31] Z. Lan, R. Daga, R. Whitehouse, S. McCarthy, D. Schmidt, Structure–properties relations in flexible polyurethane foams containing a novel bio-based crosslinker, Polymer 55 (2014) 2635–2644, https://doi.org/10.1016/j.polymer.2014.03.061.
[32] H. Li, J. Sun, C. Wang, S. Liu, D. Yuan, X. Zhou, J. Tan, L. Stubbs, C. He, High modulus, strength, and toughness polyurethane elastomer based on unmodified lignin, ACS Sus. Chem. Eng. 5 (2017) 7942–7949, https://doi.org/10.1021/acssuschemeng.7b01481.
[33] J. Du, H. Wang, Z. Huang, X. Liu, X. Yin, J. Wu, W. Lin, X. Lin, G. Yi, Construction and mechanism study of lignin-based polyurethane with high strength and high self-healing properties, Int. J. Biol. Macromol. 248 (2023) 125925, https://doi.org/10.1016/j.ijbiomac.2023.125925.
[34] Y. Wang, C.E. Wyman, C.M. Cai, A.J. Ragauskas, Lignin-based polyurethanes from unmodified kraft lignin fractionated by sequential precipitation, ACS Appl. Polym. Mater. 1 (2019) 1672–1679, https://doi.org/10.1021/acsapm.9b00228.
[35] S. Laurichesse, C. Huilleta, L. Avérous, Original polyols based on organosolv lignin and fatty acids: new bio-based building blocks for segmented polyurethane synthesis, Green Chem. 16 (2014) 3958–3970, https://doi.org/10.1039/C4GC00596A.
[36] T. He, W. Zhu, M. Liu, X. Tian, F. Chen, Production of polyurethane elastomer from highly reactive acetic acid lignin-derived polyols with reduced molecular weights, Biofuels Bioprod. Biorefin. 15 (2021) 1110–1125, https://doi.org/10.1002/bbb.2226.
[37] D. Sun, J. Mo, W. Liu, N. Yan, X. Qiu, Ultra-strong and tough bio-based polyester elastomer with excellent photothermal shape memory effect and degradation performance, Adv. Funct. Mater. 34 (2024) 2403333, https://doi.org/10.1002/adfm.202403333.
[38] D. Meng, H. Wang, Y. Li, J. Liu, J. Sun, X. Gu, H. Wang, S. Zhang, Constructing lignin based nanoparticles towards flame retardant thermoplastic polyurethane composites with improved mechanical and oxidation resistant properties, Int. J. Biol. Macromol. 253 (2023) 126570, https://doi.org/10.1016/j.ijbiomac.2023.126570.
[39] T. He, F. Chen, W. Zhu, N. Yan, Functionalized lignin nanoparticles for producing mechanically strong and tough flame-retardant polyurethane elastomers, Int. J. Biol. Macromol. 209 (2022) 1339–1351, https://doi.org/10.1016/j.ijbiomac.2022.04.089.
[40] M. Puyadena, P. Widsten, T. Wirtanen, M. Kellock, G. Ortega, A. Mugica, E. Matxinandiarena, I. Etxeberria, L. Martin, A. Agirre, A. Barrio, A. Gonzalez, L. Irusta, Phosphorus-containing lignin intermediates as reactive bio-based flame-retardants for polyurethane and acrylic coatings for wood, Ind. Crop Prod. 220 (2024) 119261, https://doi.org/10.1016/j.indcrop.2024.119261.
[41] V. Carretier, J. Delcroix, M.F. Pucci, P. Rublon, J.M. Lopez-Cuesta, Influence of sepiolite and lignin as potential synergists on flame retardant systems in polylactide (PLA) and polyurethane elastomer (PUE), Materials 13 (2020) 2450, https://doi.org/10.3390/ma13112450.
[42] J. Liu, J. Dai, S. Wang, Y. Peng, L. Cao, X. Liu, Facile synthesis of bio-based reactive flame retardant from vanillin and guaiacol for epoxy resin, Compos. Part B-Eng. 190 (2020) 107926, https://doi.org/10.1016/j.compositesb.2020.107926.
[43] B. Hou, X. Shan, B. Li, Y. Zhang, B. Xu, Z. Chen, Q. Cui, J. Li, Phosphorus-nitrogen-containing flame-retardant plasticizers derived from L-lactic acid for poly (lactic acid) improved toughness, flame retardancy and crystallization, Chem. Eng. J. 500 (2024) 157143, https://doi.org/10.1016/j.cej.2024.157143.
[44] N. Safronava, R.E. Lyon, S. Crowley, S.I. Stoliarov, Effect of moisture on ignition time of polymers, Fire Technol. 51 (2014) 1093–1112, https://doi.org/10.1007/s10694-014-0434-1.
[45] Y. Ni, Q. Li, L. Chen, W. Wu, Z. Qin, Y. Zhang, L. Chen, X. Wang, Y. Wang, Semi-aromatic copolyesters with high strength and fire safety via hydrogen bonds and π-π stacking, Chem. Eng. J. 374 (2019) 694–705, https://doi.org/10.1016/j.cej.2019.05.212.
[46] M. Wan, C. Shi, X. Qian, Y. Qin, J. Jing, F. H. Che, J. Li Ren, B. Yu, K. Zhou, Design of novel double-layer coated ammonium polyphosphate and its application in flame retardant thermoplastic polyurethanes, Chem. Eng. J. 459 (2023) 141448, https://doi.org/10.1016/j.cej.2023.141448.
[47] H. Duan, Y. Chen, S. Ji, R. Hu, H. Ma, A novel phosphorus/nitrogen-containing polycarboxylic acid endowing epoxy resin with excellent flame retardance and mechanical properties, Chem. Eng. J. 375 (2019) 121916, https://doi.org/10.1016/j.cej.2019.121916.
[48] S. Huo, S. Yang, J. Wang, J. Cheng, Q. Zhang, Y. Hu, G. Ding, Q. Zhang, P. Song, H. Wang, A liquid phosphaphenanthrene-derived imidazole for improved flame retardancy and smoke suppression of epoxy resin, ACS Appl. Pol. Mater. 2 (2020) 3566–3575, https://doi.org/10.1021/acsapm.0c00577.
[49] Z. Chi, Z. Guo, Z. Xu, M. Zhang, M. Li, L. Shang, Y. Ao, A DOPO-based phosphorus-nitrogen flame retardant bio-based epoxy resin from diphenolic acid: synthesis, flame-retardant behavior and mechanism, Polym. Degrad. Stab. 176 (2020) 109151, https://doi.org/10.1016/j.polymdegradstab. 2020.109151.
[50] P. Gnanasekar, H. Chen, N. Tratnik, M. Feng, N. Yan, Enhancing performance of phosphorus containing vanillin-based epoxy resins by P–N non-covalently functionalized graphene oxide nanofillers, Compos. Part B-Eng. 207 (2021) 108585, https://doi.org/10.1016/j.compositesb.2020.108585.
[51] J. Chen, Z. Liu, S. Qiu, Y. Li, J. Sun, H. Li, X. Gu, S. Zhang, A new strategy for the preparation of polylactic acid composites with flame retardancy, UV resistance, degradation, and recycling performance, Chem. Eng. J. 472 (2023) 145000, https://doi.org/10.1016/j.cej.2023.145000.